H1-prelim-17-031
March 28, 2017

https://www-h1.desy.de/publications/H1preliminary.short_list.html

Determination of the strong coupling constant $\alpha_s(m_Z)$ in next-to-next-to-leading order QCD using H1 jet cross section measurements

H1 Collaboration

and

V. Bertone, J. Currie, T. Gehrmann, C. Gwenlan, A. Huss, J. Niehues, M. Sutton

Abstract

The strong coupling constant $\alpha_s(m_Z)$ is determined in a fit of next-to-next-to-leading order (NNLO) QCD predictions to inclusive jet and dijet cross section measurements by H1. Using H1 inclusive jet and dijet data together, the value of the strong coupling constant is determined to $\alpha_s(m_Z) = 0.1157(6)_{\rm exp}(^{+31}_{-26})_{\rm theo}$.

1 Introduction and H1 jet cross section measurements

Cross sections for jet production in electron-proton collisions have been measured by the H1 experiment at HERA at different center-of-mass energies and during different data taking periods. For the present analysis, we consider inclusive jet and dijet cross sections. A summary of the individual measurements is given in table 1. Common to all data sets,

Kinematic range of H1 jet data

Data set [Ref.]	$\sqrt{s}$ [GeV]	int. $\mathcal{L}$ [pb^{-1}]	DIS kinematic range	Inclusive jets	Dijets $n_{\text{jets}} \geq 2$
300 GeV [1]	300	33	$150 < Q^2 < 5000\,\text{GeV}^2$ $0.2 < y < 0.6$	$7 < P_{\text{T}}^{\text{jet}} < 50\,\text{GeV}$	$P_{\text{T}}^{\text{jet}} > 7\,\text{GeV}$ $8.5 < \langle P_{\text{T}} \rangle < 35\,\text{GeV}$
HERA-I [2]	319	43.5	$5 < Q^2 < 100\,\text{GeV}^2$ $0.2 < y < 0.7$	$5 < P_{\text{T}}^{\text{jet}} < 80\,\text{GeV}$	$5 < P_{\text{T}}^{\text{jet}} < 50\,\text{GeV}$ $5 < \langle P_{\text{T}} \rangle < 80\,\text{GeV}$ $(\langle P_{\text{T}} \rangle > 7\,\text{GeV})^*$ $m_{12} > 18\,\text{GeV}$
HERA-I [3]	319	65.4	$150 < Q^2 < 15000\,\text{GeV}^2$ $0.2 < y < 0.7$	$5 < P_{\text{T}}^{\text{jet}} < 50\,\text{GeV}$	–
HERA-II [4]	319	290	$5.5 < Q^2 < 80\,\text{GeV}^2$ $0.2 < y < 0.6$	$4.5 < P_{\text{T}}^{\text{jet}} < 50\,\text{GeV}$	$P_{\text{T}}^{\text{jet}} > 4\,\text{GeV}$ $5 < \langle P_{\text{T}} \rangle < 50\,\text{GeV}$
HERA-II [5, 4]	319	351	$150 < Q^2 < 15000\,\text{GeV}^2$ $0.2 < y < 0.7$	$5 < P_{\text{T}}^{\text{jet}} < 50\,\text{GeV}$	$5 < P_{\text{T}}^{\text{jet}} < 50\,\text{GeV}$ $7 < \langle P_{\text{T}} \rangle < 50\,\text{GeV}$ $m_{12} > 16\,\text{GeV}$

Table 1: Summary of the kinematic range of the studied inclusive jet and dijet data sets. In case of the HERA-I low-Q^2 data set, an additional cut of $\langle P_{\text{T}} \rangle > 7\,\text{GeV}$ was imposed for this analysis in order to avoid infrared sensitive regions of the NNLO calculations.

jets are defined in the Breit frame using the k_t clustering algorithm [6] with a resolution parameter of $R = 1$. The jets are required to be contained in the pseudorapidity range $-1 < \eta_{\text{lab}}^{\text{jet}} < 2.5$ in the laboratory frame. The data sets are subdivided into so-called low-Q^2 ($Q^2 \lesssim 100\,\text{GeV}^2$) and high-$Q^2$ sets ($Q^2 \gtrsim 150\,\text{GeV}^2$) , where the scattered lepton is identified in different experimental devices.

Inclusive jet cross sections are measured double-differentially as functions of Q^2 and the jet transverse momentum in the Breit frame, $P_{\text{T}}^{\text{jet}}$, where the phase space is constrained by Q^2, the inelasticity y, $\eta_{\text{lab}}^{\text{jet}}$ and $P_{\text{T}}^{\text{jet}}$, as specified in table 1.

Dijet cross sections are measured double-differentially as functions of Q^2 and $\langle P_{\text{T}} \rangle$. The latter is defined by the transverse momenta of the two leading jets as $\langle P_{\text{T}} \rangle = (P_{\text{T}}^{\text{jet1}} + P_{\text{T}}^{\text{jet2}})/2$. For dijets at least two jets must be identified in the $\eta_{\text{lab}}^{\text{jet}}$-range above a certain $P_{\text{T}}^{\text{jet}}$ threshold. In order to avoid regions of phase space, where the predictions exhibit an infrared sensitivity, the phase space definitions impose asymmetric cuts on the transverse momenta of the two leading jets [7]. Such an asymmetric cut is also given by a constraint

on $\langle P_{\mathrm{T}} \rangle$. In case of the HERA-I low-Q^2 dijet cross sections, an additional cut of $\langle P_{\mathrm{T}} \rangle > 7\,\mathrm{GeV}$ is therefore applied for this work.

To each data bin a typical scale value $\tilde{\mu}$ is assigned. It is estimated from the averages of the logarithmic values of the bin boundaries together with eq. (2). As the NNLO calculations are performed with five massless flavors, and effects from heavy quark masses may become important at lower scales, the data are constrained further to $\tilde{\mu} > 2m_b$, with m_b being the mass of the b-quark.

2 The α_s-dependence of jet cross section predictions

The cross sections for inclusive jet and dijet production for a given phase space interval i ('bin') are given through the application of the factorisation theorem as

$$\sigma_i = \sum_{n=1}^{\infty} \sum_{k=g,q,\overline{q}} \int dx f_k(x, \mu_F) \hat{\sigma}_{i,k}^{(n)}(x, \mu_R, \mu_F) \cdot c_{\mathrm{had}} \ , \tag{1}$$

where f_k denotes the parton density functions of the proton (PDF) for all parton flavors k, $\hat{\sigma}$ denotes the partonic cross section calculated perturbatively to order n, and c_{had} are non-perturbative correction factors to account for hadronisation effects. The renormalisation and factorisation scales are chosen to be

$$\mu_R^2 = \mu_F^2 = Q^2 + P_T^2 \ , \tag{2}$$

where P_T denotes $P_{\mathrm{T}}^{\mathrm{jet}}$ in case of inclusive jet cross sections and $\langle P_{\mathrm{T}} \rangle$ for dijet cross sections. This choice provides reasonable hard scales in both kinematical limits ($Q^2 \to 0\,\mathrm{GeV}^2$ and $P_T \to 0\,\mathrm{GeV}$).

The NNLO inclusive jet and dijet cross sections as a function of a multiplicative factor applied to the renormalisation and factorisation scales is studied in figure 1. Implications of the scale choice on the fit results are studied in more detail below.

The PDF, f, is provided by the NNPDF3.0 PDF set [8], which was obtained with a value of $\alpha_{\mathrm{s}}(m_{\mathrm{Z}}) = 0.118$.

The sensitivity of jet cross section predictions, σ, to the strong coupling constant is given on the one hand by the hard coefficients $\hat{\sigma}$. Their α_{s}-dependence is explicitly present in terms of the perturbative expansion in orders of $\alpha_s^{(n)}$:

$$\hat{\sigma}_{i,k}^{(n)} = \alpha_s^n(\mu_R) \tilde{\sigma}_{i,k}^{(n)}(x, \mu_R, \mu_F) \ , \tag{3}$$

where for jet cross sections the lowest non-zero order is $n = 1$. These coefficients are calculated up to next-to-next-to-leading order (NNLO), i.e. up to $\mathcal{O}(\alpha_{\mathrm{s}}^3)$, using the program NNLOJET [7, 9], and include the jet function as well as the phase space integration.

On the other hand, the PDFs exhibit a dependence on $\alpha_{\mathrm{s}}(m_{\mathrm{Z}})$, which is defined by the factorisation theorem and can be schematically written as

$$\frac{\partial f}{\partial \alpha_{\mathrm{s}}} = \frac{\mathcal{P} \otimes f}{\beta} \ , \tag{4}$$

with $\mathcal{P}$ being the QCD splitting kernels and β are the QCD β-functions. Through integration, a PDF for a given value of $\alpha_s(m_Z)$, can thus be translated to any other value of $\alpha_s(m_Z)$, once the splitting kernels have been calculated perturbatively. Alternatively, one finds an equivalent solution to the explicit integration of eq. (4), by re-evaluating the PDFs at a suitable value of μ_F. By doing so, no recalculation of the splitting kernels is required, since the $\alpha_s(m_Z)$-dependence of the PDF is fully represented by the μ_F-dependence of the PDFs alone, and thus the $\alpha_s(m_Z)$-dependence of the PDFs fully factorise. In our analysis, we employ this factorised approach. However, as the employed PDFs have all been determined in the DGLAP evolution approach, we implicitly employ an integration of eq. (4) in order to account for the α_s-dependence of the PDFs, and the evolution kernels have been calculated in NNLO (which are formally of $\mathcal{O}(\alpha_s^3)$),

The NNLO inclusive jet and dijet cross section predictions on the strong coupling constant $\alpha_s(m_Z)$ is studied in figure 2, where the two contributions from $\alpha_s(m_Z)$ (see eq. (3) and eq. (4)) are separately identified for illustrative purposes.

3 Fit methodology

The value of the strong coupling constant $\alpha_s(m_Z)$ at the reference value of the Z-boson mass, $m_Z = 91.1876\,\text{GeV}$, is determined in a fit of the theory predictions (eq. (1)) with $\alpha_s(m_Z)$ being the only fit parameter and the value of $\alpha_s(\mu_R)$ is obtained by the solutions of the QCD renormalisation group equations [10]. The goodness of fit-quality, which is also subject to the minimisation algorithm, is judged by a χ^2-quantity defined as

$$\chi^2 = \sum_{i,j} \log \frac{\varsigma_i}{\sigma_i} (V_{\text{exp}} + V_{\text{had}} + V_{\text{PDF}})^{-1}_{ij} \log \frac{\varsigma_j}{\sigma_j} \ , \tag{5}$$

where the sum (i, j) runs over all data points (ς_i), and the covariance matrix expresses the relative uncertainties of the data (exp), hadronisation correction factors (had) and the PDFs. The uncertainty on the hadronisation corrections are provided together with the data in the H1 publications, and the PDF uncertainties are obtained from the respective PDF set. This χ^2-expression can be equivalently expressed in terms of nuisance parameters for correlated systematic uncertainties and PDF eigenvectors.

Correlations of the experimental uncertainties are considered whenever applicable, and more details are found in the respective H1 publications.

Several fits are performed and values of the strong coupling constant $\alpha_s(m_Z)$ are determined separately from

- each data set as specified in table 1,
- all inclusive jet data points
- all dijet data points,
- all H1 jet data taken together, denoted as 'H1 jets' in the following,
- to data points with comparable values of $\tilde{\mu}$ and
- to data points above a certain value of $\tilde{\mu}$.

In the case of fits to 'H1 jets', dijet data from the HERA-I running period are not considered, since the statistical correlations to the respective inclusive jet data are not available.

Besides a linear error propagation of the experimental uncertainties, several uncertainties on the theoretical predictions σ_i are considered. A scale uncertainty, which accounts for contributions beyond NNLO are estimated by variations of the scales by factors of 0.5 and 2. The PDF uncertainty and the hadronisation uncertainties are obtained by repeating the fit with V_{PDF} or V_{had} excluded in the χ^2-definition. PDF sets other than the NNPDF3.0 set, as well as PDFs obtained using different values of $\alpha_{\mathrm{s}}(m_{\mathrm{Z}})$, are studied and considered for the uncertainty estimation. The 'PDFSet uncertainty' is defined as half of the maximum difference of the results from fits using the ABMP [11], CT14 [12], HERAPDF2.0 [13], MMHT [14] or NNPDF3.0 PDF set [8]. The 'PDFα_{s} uncertainty' is defined as half of the difference of the results, when the fits are repeated with PDFs which were obtained with $\alpha_{\mathrm{s}}(m_{\mathrm{Z}})$-values differing by 0.004.

The fits are performed using the Alpos fitting framework, where we employ the TMinuit minimisation algorithms [15, 16]. The PDFs are obtained through the LHAPDF package [17]. The hard coefficients are calculated using the program NNLOJET [18], which is interfaced to APPLgrid [19] and fastNLO [20]. The α_{s}-evolution is calculated using the CRunDec code [10]. The μ_F-translation for the α_{s}-dependence of the PDFs is calculated using the APFEL package [21].

4 Studies and results

First, the sensitivity of the predictions to $\alpha_{\mathrm{s}}(m_{\mathrm{Z}})$ and the consistency of the calculations are studied. The two distinct appearances of $\alpha_{\mathrm{s}}(m_{\mathrm{Z}})$ in eq. (1) in the PDFs, $\alpha_{\mathrm{s}}^{f}(m_Z)$, and the hard coefficients, $\alpha_{\mathrm{s}}^{\hat{\sigma}}(m_Z)$, are separately identified, writing schematically:

$$\sigma_i = f(\alpha_{\mathrm{s}}^{f}(m_Z)) \otimes \hat{\sigma}_k(\alpha_{\mathrm{s}}^{\hat{\sigma}}(m_Z)) \cdot c_{\mathrm{had}} \ . \tag{6}$$

Fits with two free parameters are performed separately for data points with $\tilde{\mu}$ below 15 GeV and for data points with $\tilde{\mu}$ above 15 GeV . The results are displayed for inclusive jets and dijets in figure 3. Good consistency is found for the two fitted values of $\alpha_{\mathrm{s}}(m_{\mathrm{Z}})$ of all four fits studied, and it is found that the predominant sensitivity arises from the hard coefficients. Furthermore, it is found that the two separately identified $\alpha_{\mathrm{s}}(m_{\mathrm{Z}})$ appearances are negatively correlated, which in total increases the sensitivity of the data to $\alpha_{\mathrm{s}}(m_{\mathrm{Z}})$. However, for larger values of $\alpha_{\mathrm{s}}(m_{\mathrm{Z}})$, this anti-correlation is reduced for higher values of $\tilde{\mu}$ and finally becomes positive for high values of $\tilde{\mu}$, which was expected already from figure 2.

Values of $\alpha_{\mathrm{s}}(m_{\mathrm{Z}})$ are determined for alternative choices of the renormalisation and factorisation scales for the NNLO calculations and results are displayed in figure 4 for fits to inclusive jet and to dijet cross sections, respectively, and for fits to H1 jets in figure 5. These figures display further results from fits, which employ hard coefficients $\hat{\sigma}$ calculated only in NLO precision[1]. It is found, that in general the NNLO calculations exhibit a

[1]For better comparison, the identical scale choice and the same PDF as for the NNLO fits were used.

reduction of the sensitivity to the scale choice, as well as to scale variations, which is expressed by the size of the scale uncertainty.

The dependence of the fit results on the multiplicative variations of the renormalisation and factorisation scales in the NNLO calculations are studied. The results are displayed in figure 6 for fits to inclusive jet and to dijet cross sections, respectively, and for fits to H1 jets in figure 7. It is found, that the renormalisation and the factorisation scale variations have a significant impact to the result, but variations by large multiplicative factors yield to an increase of χ^2/n_{dof}.

Values of $\alpha_{\mathrm{s}}(m_{\mathrm{Z}})$ are determined for alternative choices of the PDF set, and for alternative choices of $\alpha_{\mathrm{s}}(m_{\mathrm{Z}})$-values which were used for the determination of the PDFs. The results to inclusive jet and dijet cross sections are displayed in figure 8 and H1 jets in figure 9. Consistency is found for the studied PDF sets. A significant correlation of the fitted value of $\alpha_{\mathrm{s}}(m_{\mathrm{Z}})$ to the $\alpha_{\mathrm{s}}(m_{\mathrm{Z}})$-value which was employed for the PDF extraction is found. This correlation is considerably higher than was reported in previous analyses, where different fitting methodologies were employed.

The a priori chosen PDF set NNPDF3.0 and the a priori chosen scale definition of $\mu_R^2 = \mu_F^2 = Q^2 + P_T^2$ provide an overall good agreement of theory to data.

The running of the strong coupling constant is tested by fits to groups of data points[2] with comparable values of $\tilde{\mu}$. The results for fits to inclusive jet and to dijet cross sections, as well as to H1 jets, are displayed for ten selected intervals of $\tilde{\mu}$ in figure 10. In order to illustrate the running of the strong coupling constant for that figure, the fit values of $\alpha_{\mathrm{s}}(m_{\mathrm{Z}})$ are translated (back) to $\alpha_{\mathrm{s}}(\tilde{\mu})$, i.e. to a representative value of $\tilde{\mu}$ of that $\tilde{\mu}$-interval. Thus, for that study, the assumption of the running is only implied over the very limited range of a given $\tilde{\mu}$-range. Consistency is found for the fits to inclusive jet, to dijet, and to H1 jet data, and the assumptions of the running of the strong coupling is confirmed in the tested range of approximately 7–90 GeV .

The values obtained from fits to H1 jets are compared to other data [22, 23, 24, 25, 26] in figure 11, and consistency to other extractions is found, for ranges where other data points are available.

In order to study the dependence of the NNLO scale uncertainty on the scale of the data points, the fits to inclusive jet and to dijet cross sections are repeated for all data points which fulfill a certain minimum value of $\tilde{\mu}$. The resulting experimental, scale and theory uncertainty[3] are displayed in figure 12. As expected the experimental uncertainty increases when increasing the cut on $\tilde{\mu}$ as fewer data points are considered in the fit. The scale uncertainty, which dominates the theory uncertainty, remains almost unchanged as a function of that cut.

The results of the fits to the individual data sets are summarised in figure 13, where also the results of the fits to all inclusive jet and to all dijet data simultaneously, as well as to the H1 jets, are displayed. The $\alpha_{\mathrm{s}}(m_{\mathrm{Z}})$-values from the inclusive jet cross sections

[2]These fits do not impose the cut $\tilde{\mu} > 2m_b$.

[3]The theory uncertainty is defined as the quadratic sum of the PDF, PDFSet, PDFα_{s}, hadronisation and scale uncertainty.

are found to be overall consistent, with mentionable differences only between the HERA-I 300 GeV high-Q^2 and the HERA-I low-Q^2 data sets, while the first, however, exhibits large experimental uncertainties. The fit to all inclusive jet sets show excellent consistency of all data points with high experimental precision.

The $\alpha_s(m_Z)$-values from the dijet cross section appear to be consistent with the values from the respective inclusive jet data and only a noteworthy difference of the $\alpha_s(m_Z)$-values from the HERA-II data is found. However, the fit to all dijet cross sections exhibits an excellent consistency of all data points.

In general, an overall good agreement of theory and data is found and the the values of χ^2/n_{dof}, where n_{dof} denotes the number of data points employed in the fit minus one, are around unity. The fit to H1 jet data, for example, yields a value of

$$\chi^2/n_{\mathrm{dof}} = 1.03 \tag{7}$$

for 203 data points and one fit parameter $\alpha_s(m_Z)$.

The value of the strong coupling constant $\alpha_s(m_Z)$ is determined using H1 jet data and NNLO cross sections to

$$\alpha_s(m_Z) = 0.1157\,(6)_{\mathrm{exp}}\,(3)_{\mathrm{had}}\,(6)_{\mathrm{PDF}}\,(12)_{\mathrm{PDF}\alpha_s}\,(2)_{\mathrm{PDFset}}\,(^{+27}_{-21})_{\mathrm{scale}}\ . \tag{8}$$

The value is consistent with the world average value [27, 28] and with other extractions. A ratio of H1 jet cross section measurements to the NNLO predictions is displayed in figure 14. It is found, that the H1 inclusive jet and dijet data together ('H1 jets') with the NNLO QCD calcualtions tend to prefer a somewhat smaller value for $\alpha_s(m_Z)$ than the current world average value.

References

[1] **H1** Collaboration, C. Adloff *et al. Eur. Phys. J.* **C19** (2001) 289–311, arXiv:hep-ex/0010054.

[2] **H1** Collaboration, F. D. Aaron *et al. Eur. Phys. J.* **C67** (2010) 1–24, arXiv:0911.5678.

[3] **H1** Collaboration, A. Aktas *et al. Phys. Lett.* **B653** (2007) 134–144, arXiv:0706.3722.

[4] **H1** Collaboration, V. Andreev *et al.* arXiv:1611.03421.

[5] **H1** Collaboration, V. Andreev *et al. Eur. Phys. J.* **C75** no. 2, (2015) 65, arXiv:1406.4709.

[6] S. D. Ellis and D. E. Soper *Phys. Rev.* **D48** (1993) 3160–3166, arXiv:hep-ph/9305266.

[7] J. Currie, T. Gehrmann, A. Huss, and J. Niehues arXiv:1703.05977.

[8] **NNPDF** Collaboration, R. D. Ball *et al. JHEP* **04** (2015) 040, arXiv:1410.8849.

[9] J. Currie, T. Gehrmann, and J. Niehues *Phys. Rev. Lett.* **117** no. 4, (2016) 042001, arXiv:1606.03991.

[10] B. Schmidt and M. Steinhauser *Comput. Phys. Commun.* **183** (2012) 1845–1848, arXiv:1201.6149.

[11] S. Alekhin, J. Blümlein, S. Moch, and R. Placakyte arXiv:1701.05838.

[12] S. Dulat, T.-J. Hou, J. Gao, M. Guzzi, J. Huston, P. Nadolsky, J. Pumplin, C. Schmidt, D. Stump, and C. P. Yuan *Phys. Rev.* **D93** no. 3, (2016) 033006, arXiv:1506.07443.

[13] **ZEUS, H1** Collaboration, H. Abramowicz *et al. Eur. Phys. J.* **C75** no. 12, (2015) 580, arXiv:1506.06042.

[14] L. A. Harland-Lang, A. D. Martin, P. Motylinski, and R. S. Thorne *Eur. Phys. J.* **C75** no. 5, (2015) 204, arXiv:1412.3989.

[15] F. James and M. Roos *Comput. Phys. Commun.* **10** (1975) 343–367.

[16] I. Antcheva *et al. Comput. Phys. Commun.* **180** (2009) 2499–2512, arXiv:1508.07749.

[17] A. Buckley, J. Ferrando, S. Lloyd, K. Nordström, B. Page, M. Rüfenacht, M. Schönherr, and G. Watt *Eur. Phys. J.* **C75** (2015) 132, arXiv:1412.7420.

[18] A. Gehrmann-De Ridder, T. Gehrmann, E. W. N. Glover, A. Huss, and T. A. Morgan *JHEP* **07** (2016) 133.

[19] T. Carli, D. Clements, A. Cooper-Sarkar, C. Gwenlan, G. P. Salam, F. Siegert, P. Starovoitov, and M. Sutton *Eur. Phys. J.* **C66** (2010) 503–524, arXiv:0911.2985.

[20] D. Britzger, K. Rabbertz, F. Stober, and M. Wobisch, "New features in version 2 of the fastNLO project," in *Proceedings, 20th International Workshop on Deep-Inelastic Scattering and Related Subjects (DIS 2012): Bonn, Germany, March 26-30, 2012*, pp. 217–221. 2012. arXiv:1208.3641.

[21] V. Bertone, S. Carrazza, and J. Rojo *Comput. Phys. Commun.* **185** (2014) 1647–1668, arXiv:1310.1394.

[22] **Gfitter Group** Collaboration, M. Baak, J. Cúth, J. Haller, A. Hoecker, R. Kogler, K. Mönig, M. Schott, and J. Stelzer *Eur. Phys. J.* **C74** (2014) 3046, arXiv:1407.3792.

[23] **OPAL** Collaboration, G. Abbiendi *et al. Eur. Phys. J.* **C71** (2011) 1733, arXiv:1101.1470.

[24] **JADE** Collaboration, J. Schieck, S. Bethke, S. Kluth, C. Pahl, and Z. Trocsanyi *Eur. Phys. J.* **C73** no. 3, (2013) 2332, arXiv:1205.3714.

[25] G. Dissertori, A. Gehrmann-De Ridder, T. Gehrmann, E. W. N. Glover, G. Heinrich, and H. Stenzel *JHEP* **02** (2008) 040, arXiv:0712.0327.

[26] **CMS** Collaboration, S. Chatrchyan *et al. Phys. Lett.* **B728** (2014) 496–517, arXiv:1307.1907. [Erratum: Phys. Lett.B738,526(2014)].

[27] S. Bethke, "alpha s 2016," in *Proceedings, 19th International Conference in Quantum Chromodynamics (QCD 16): Montpellier, France, July 4–9, 2016*, vol. 282-284, pp. 149–152. 2017.

[28] **Particle Data Group** Collaboration, C. Patrignani *et al. Chin. Phys.* **C40** no. 10, (2016) 100001.

5 Figures

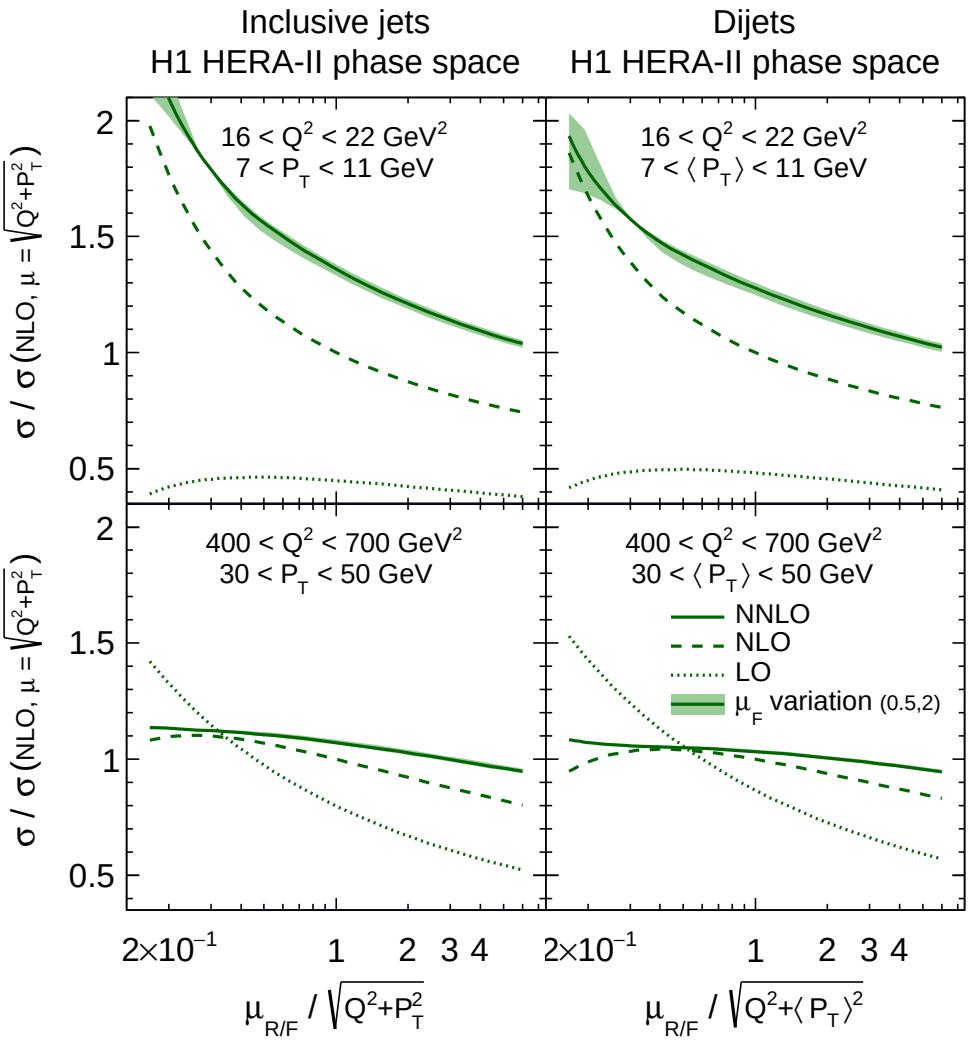

Figure 1: The cross section as a function of a multiplicative factor applied to the renormalisation and factorisation scale for four exemplary data points of the HERA-II phase space definition. The bin definitions are displayed in the respective pads. The full line shows the cross section dependence for the NNLO, the dashed line for NLO and the dotted lines for LO calculations. For better comparison, all calculations have been performed with the same PDFs set (NNPDF3.0 NNLO). All values are normalised to the NLO cross section with unity scale factor. The filled area around the NNLO calculation indicates a variation of the factorisation scale by factors of 0.5 and 2 around the chosen value for μ_R.

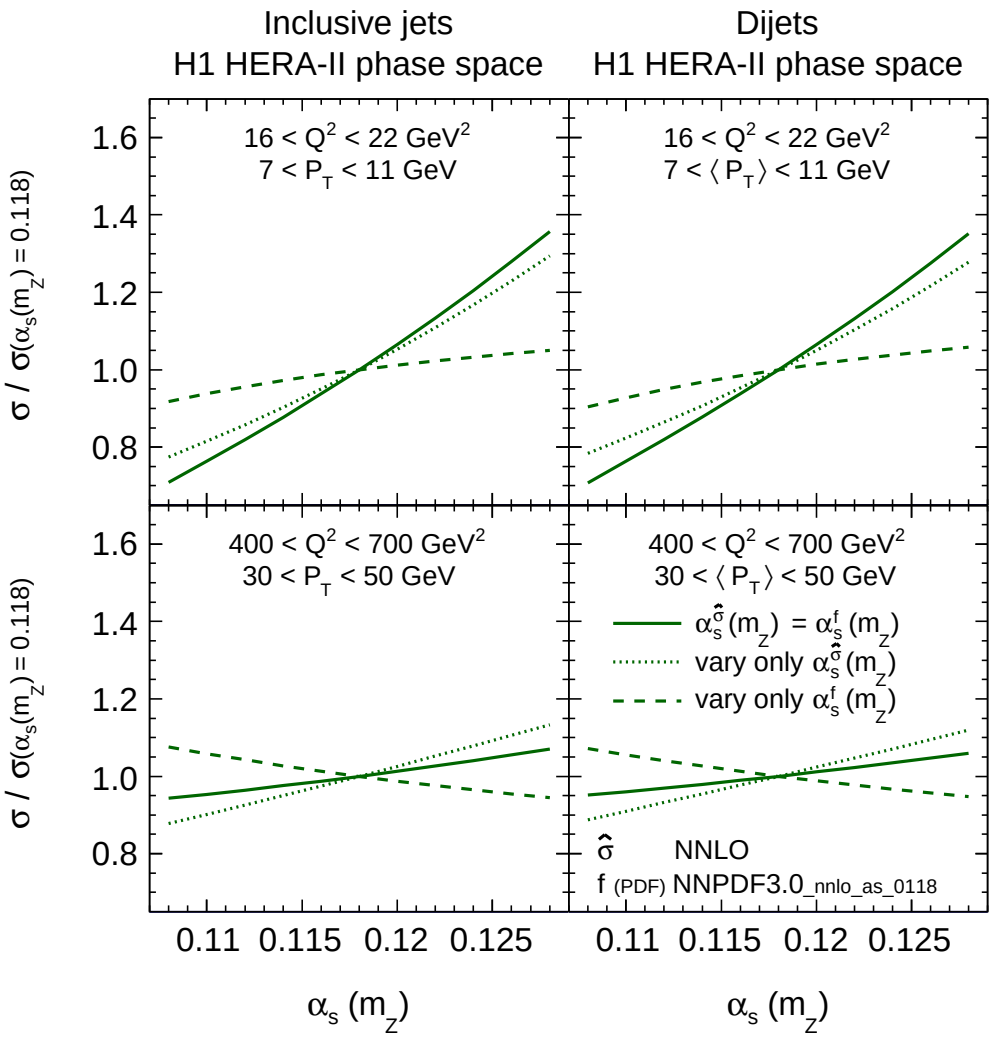

Figure 2: The cross section as a function of $\alpha_s(m_Z)$ for four exemplary data points of the HERA-II phase space definitions. The bin definitions are displayed in the respective pads. The left pads show inclusive jet cross sections, and the right pads dijet cross sections. The full line indicates the total cross section dependence as a function of $\alpha_s(m_Z)$, while the dashed lines illustrate the dependence if $\alpha_s(m_Z)$ is varied only in the hard coefficients, and the dotted line illustrates a variation only in the PDFs. The cross sections are normalised to a nominal cross section defined with $\alpha_s(m_Z) = 0.118$.

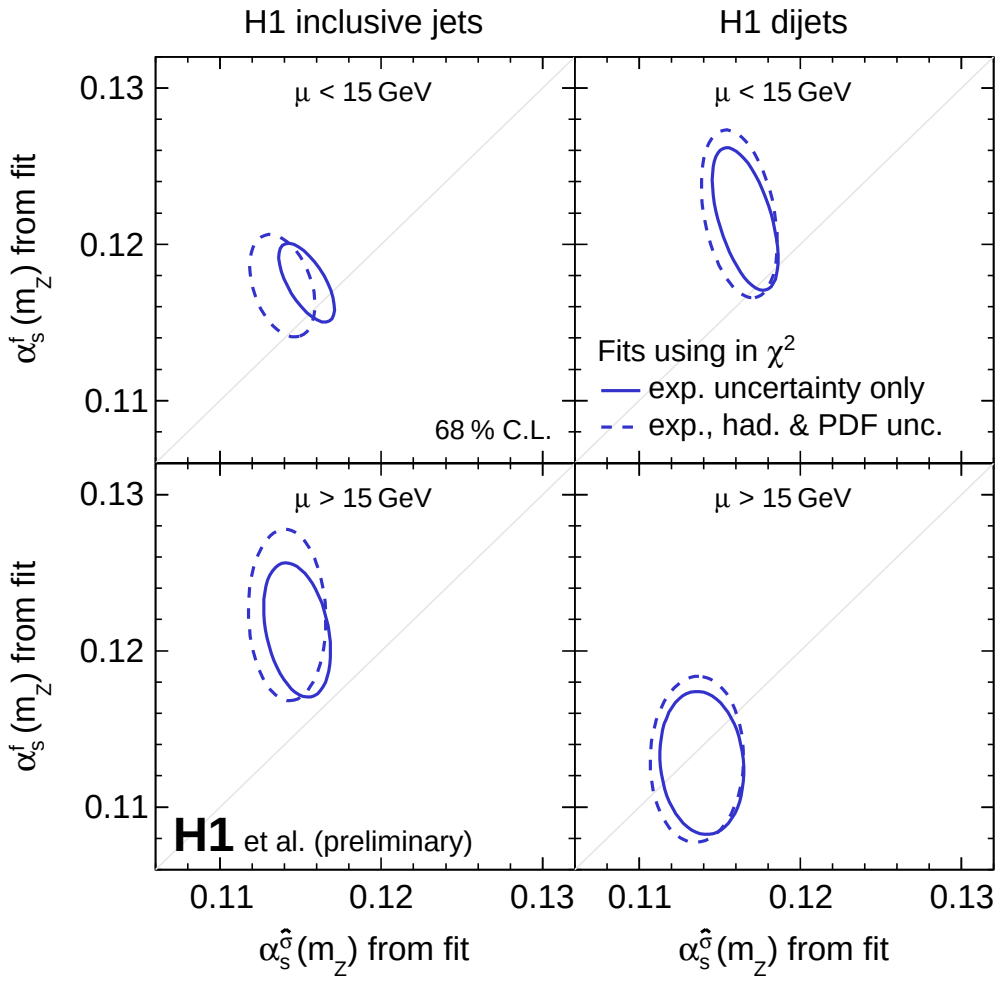

Figure 3: Results from fits to inclusive jet and dijet cross section data with two free fit parameters for $\alpha_s(m_Z)$, where the appearances of $\alpha_s(m_Z)$ in the PDFs and the hard coefficients are separately identified. The upper pads show fits to data points with $\mu_R < 15\,\text{GeV}$ and the lower pads to data points with $\mu_R > 15\,\text{GeV}$. The full line indicates the 68 % confidence level of the experimental uncertainties (where the fit is also performed with only those mentioned in the χ^2-definition), and the dashed line with experimental, hadronisation and PDF uncertainties considered in the χ^2-definition.

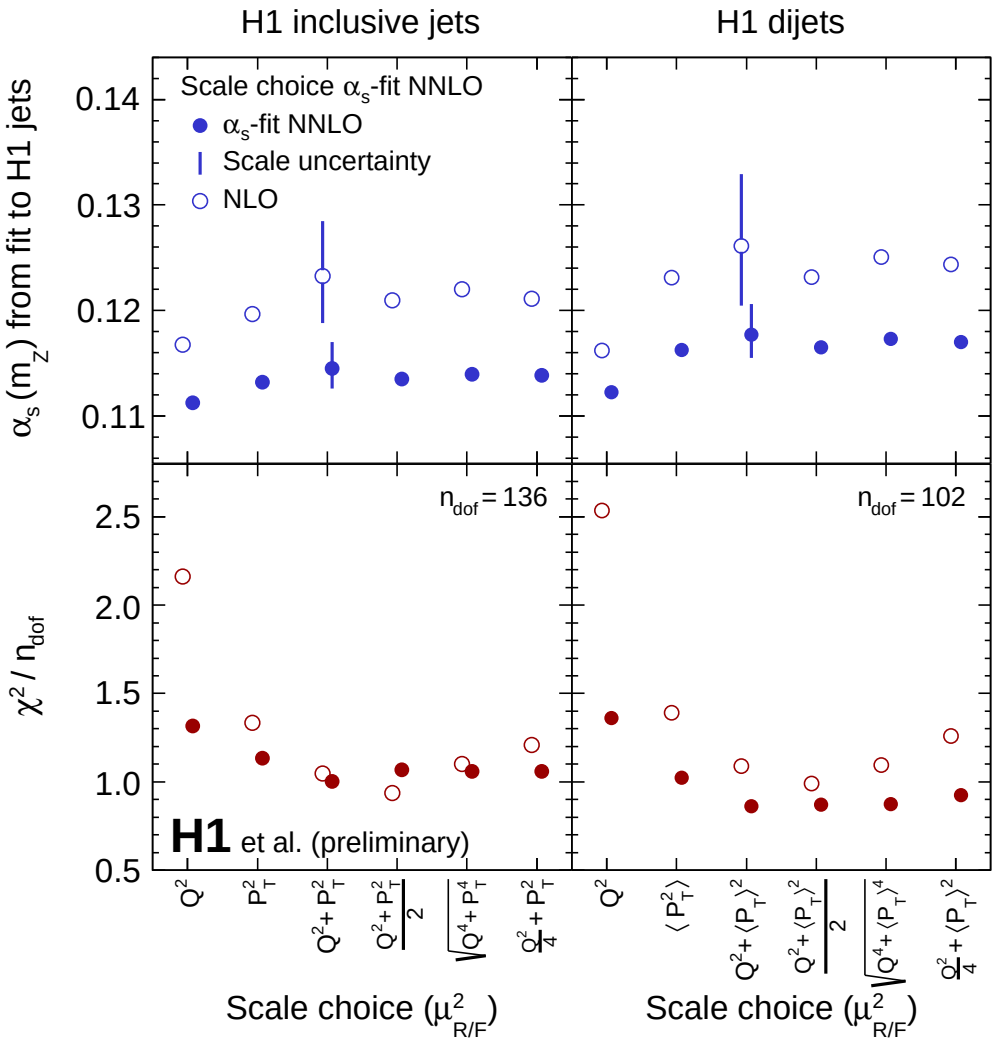

Figure 4: Dependence of the fitted values of $\alpha_s(m_Z)$ for different definitions of the renormalisation and factorisation scale. The upper pads show the fitted value of $\alpha_s(m_Z)$, and the lower pads show the values of χ^2/n_{dof}. The full circles show results obtained using NNLO matrix elements, while the open circles show results for NLO matrix elements. In the latter case, the same PDF was used as for the NNLO fit for better comparison.

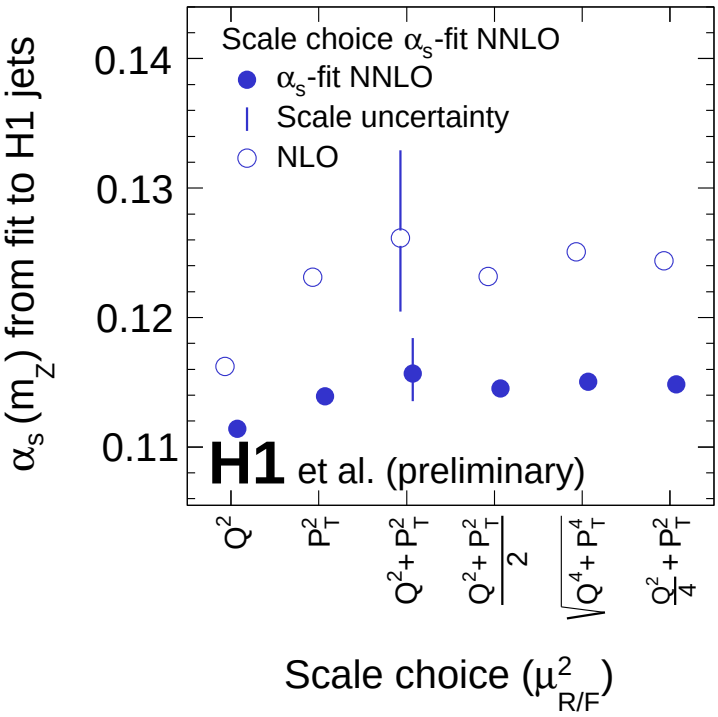

Figure 5: Same as upper pads of fig. 4, but shown for the fit to 'H1 jets'.

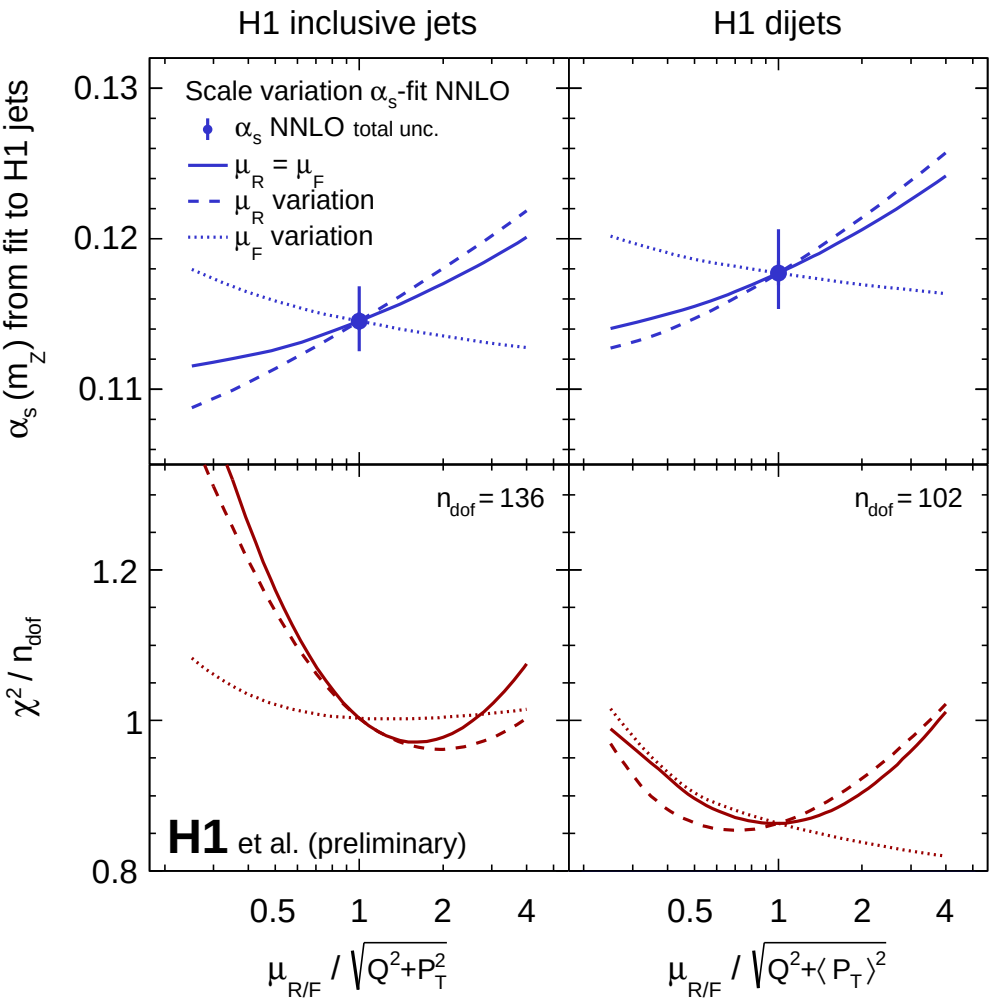

Figure 6: Dependence of the fitted values of $\alpha_s(m_Z)$ as a function of the scale factors. The upper pads show the fitted value of $\alpha_s(m_Z)$, and the lower pads show the values of χ^2/n_{dof}. The left pad shows the values for the fit to inclusive jet cross section and the right pad to dijet cross sections. The full line shows a simultaneous variation of the renormalisation and factorisation scale. The dotted line shows the results for a variation of the factorisation scale only, while the dashed line for a variation of only the renormalisation scale.

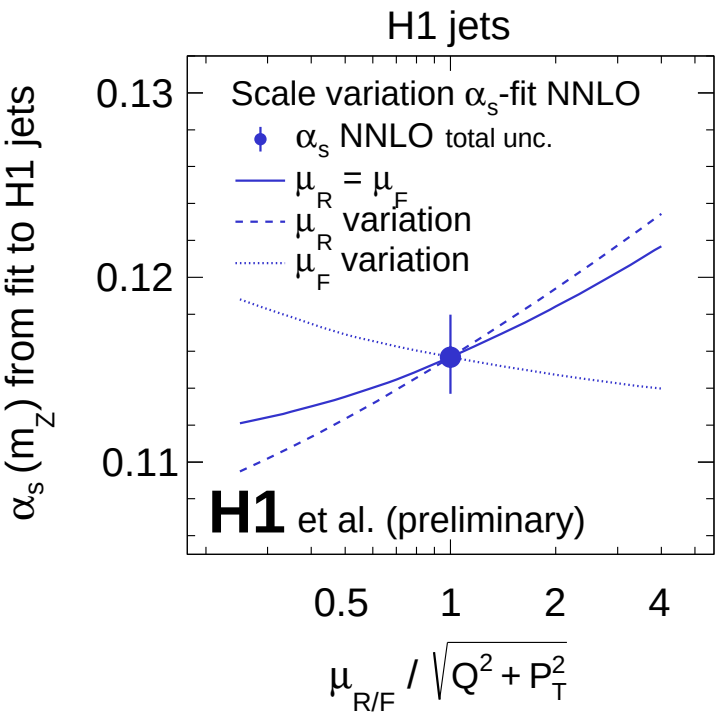

Figure 7: Same as upper pads of fig. 6, but shown for the fit to 'H1 jets'.

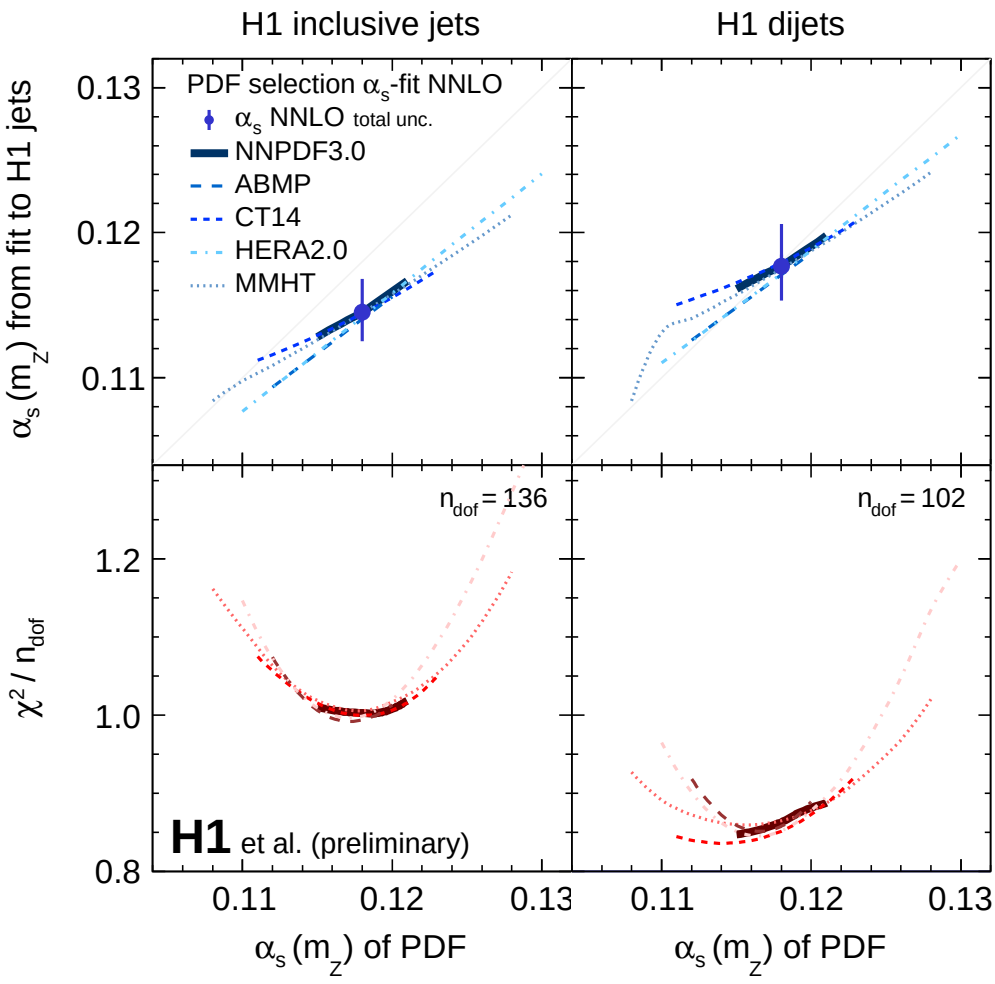

Figure 8: Dependence of the fitted values of $\alpha_s(m_Z)$ for different input PDFs to the fit. Shown are fits using the ABMP, CT14, HERAPDF2.0, MMHT and NNPDF3.0 PDF sets. For each case, the PDFs are available for different input values of $\alpha_s(m_Z)$ used at the PDF determination, and these values are displayed at the x-axis.

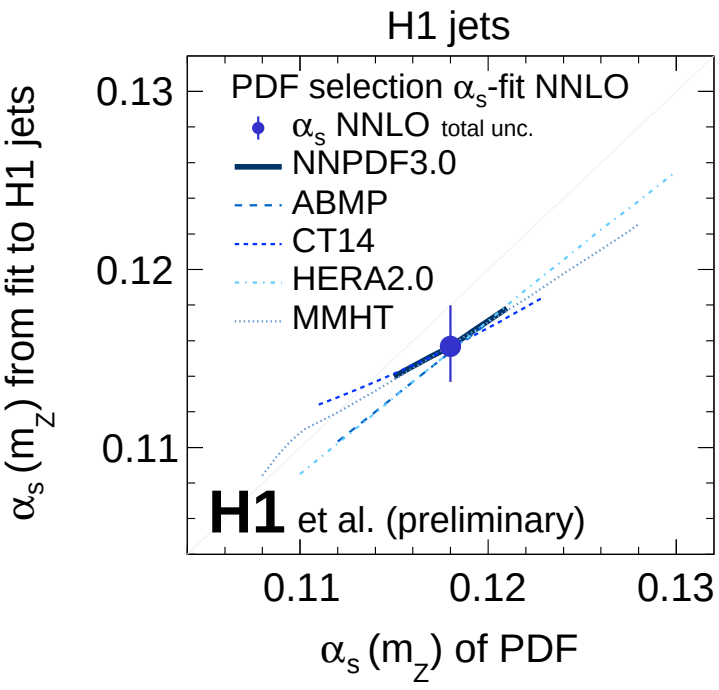

Figure 9: Same as upper pads of fig. 8, but shown for the fit to 'H1 jets'.

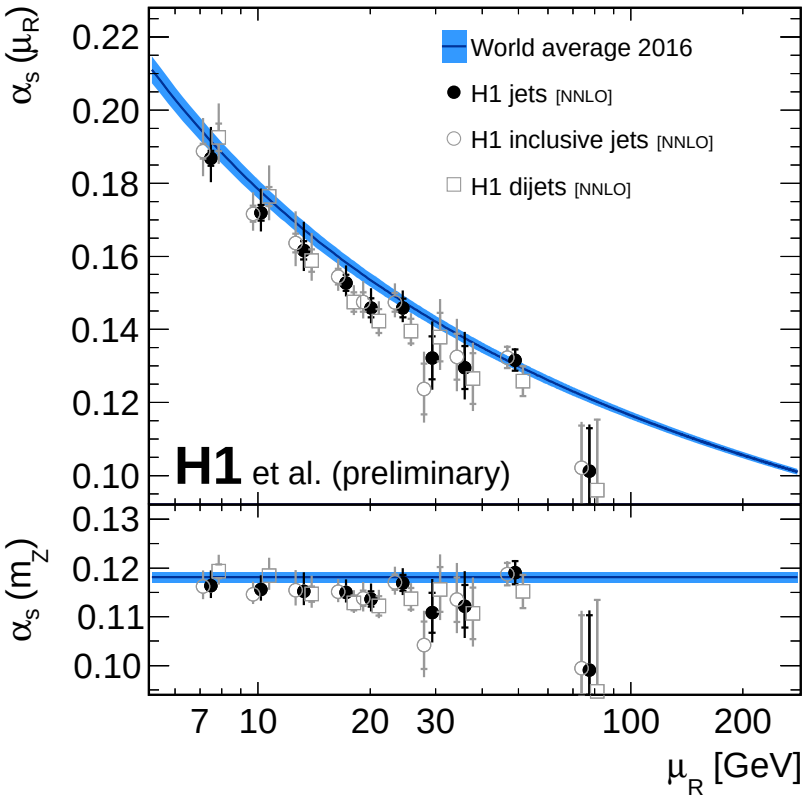

Figure 10: Results for $\alpha_s(m_Z)$ for fits to data points with similar values of μ_R. The full circles show results obtained from fits to the inclusive jet and dijet data taken together ('H1 jets'), the open circles to inclusive jet cross sections and the open boxes to dijet cross sections. For these fits, the data sets are not constrained by the requirement $\mu > 2m_b$. The values of $\alpha_s(m_Z)$ are translated to $\alpha_s(\mu_R)$, using the solution of the QCD renormalisation group equation. The data points are partially displayed with a small shift in the x-coordinate for better visibility. The inner error bars denote the experimental uncertainties alone, and the outer error bars indicate the total uncertainties.

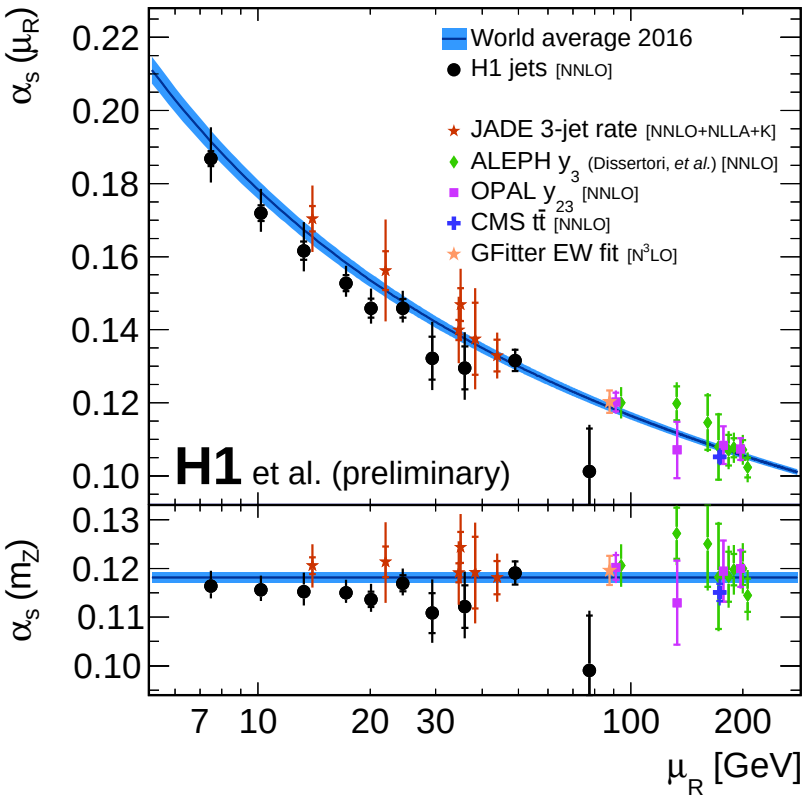

Figure 11: Results for $\alpha_s(m_Z)$ for fits to data points with similar values of μ_R, compared to values from other experiments and processes obtained using at least NNLO QCD predictions. More details are found in the caption of figure 10.

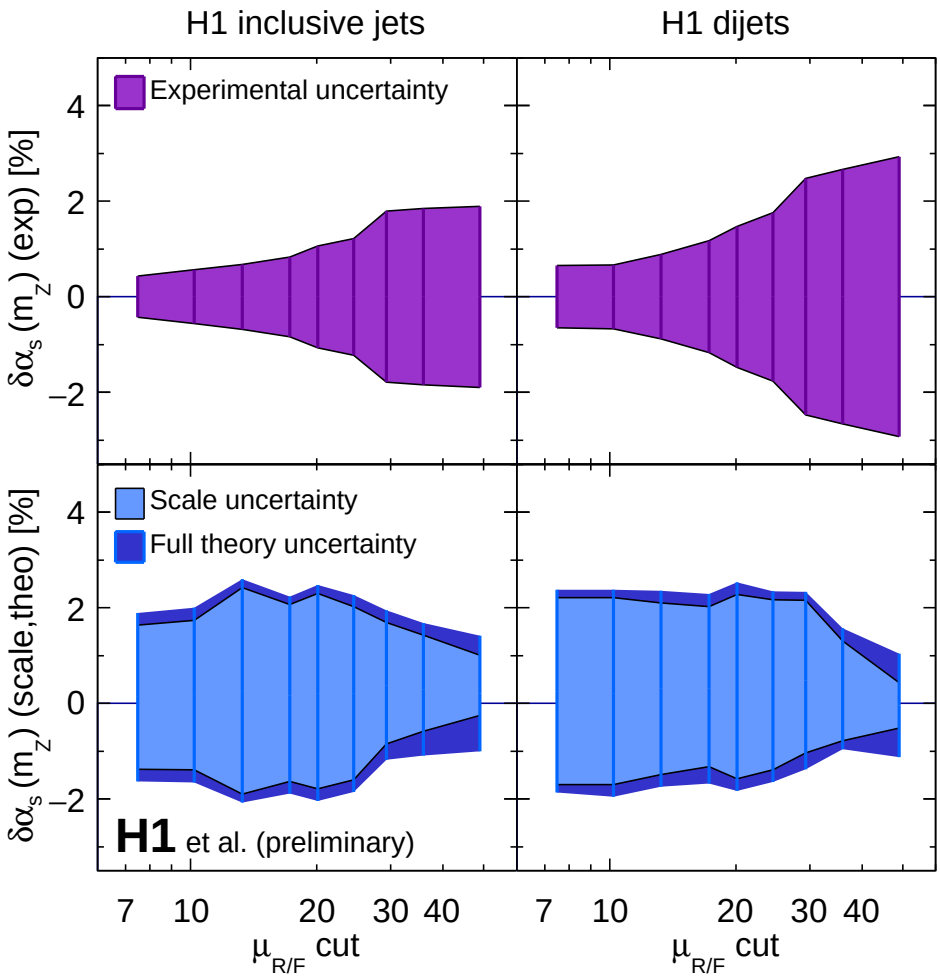

Figure 12: Resulting experimental (upper pads), scale and theory uncertainties (bottom pads), if the fit is restricted to data points above a typical value of μ. For these fits, the data sets are not constrained by the requirement $\mu > 2m_b$.

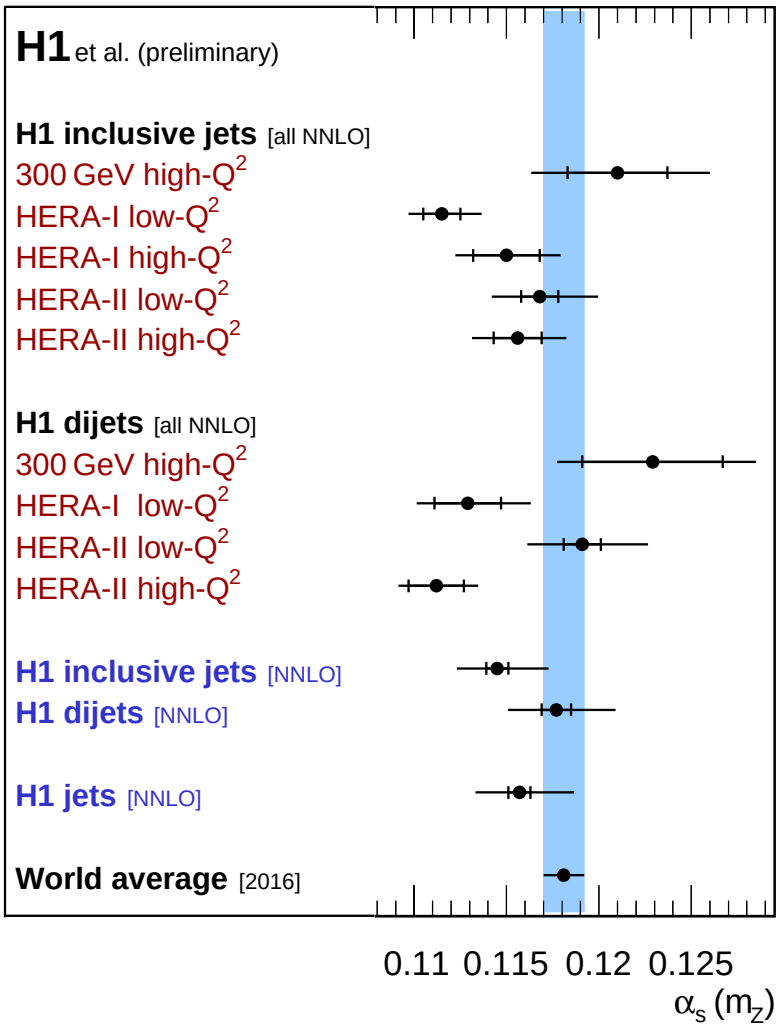

Figure 13: Summary of the values of $\alpha_s(m_Z)$ obtained from fits to the individual data sets and to fits to multiple data sets. The inner error bars indicate the experimental uncertainty and the outer error bars the total uncertainty.

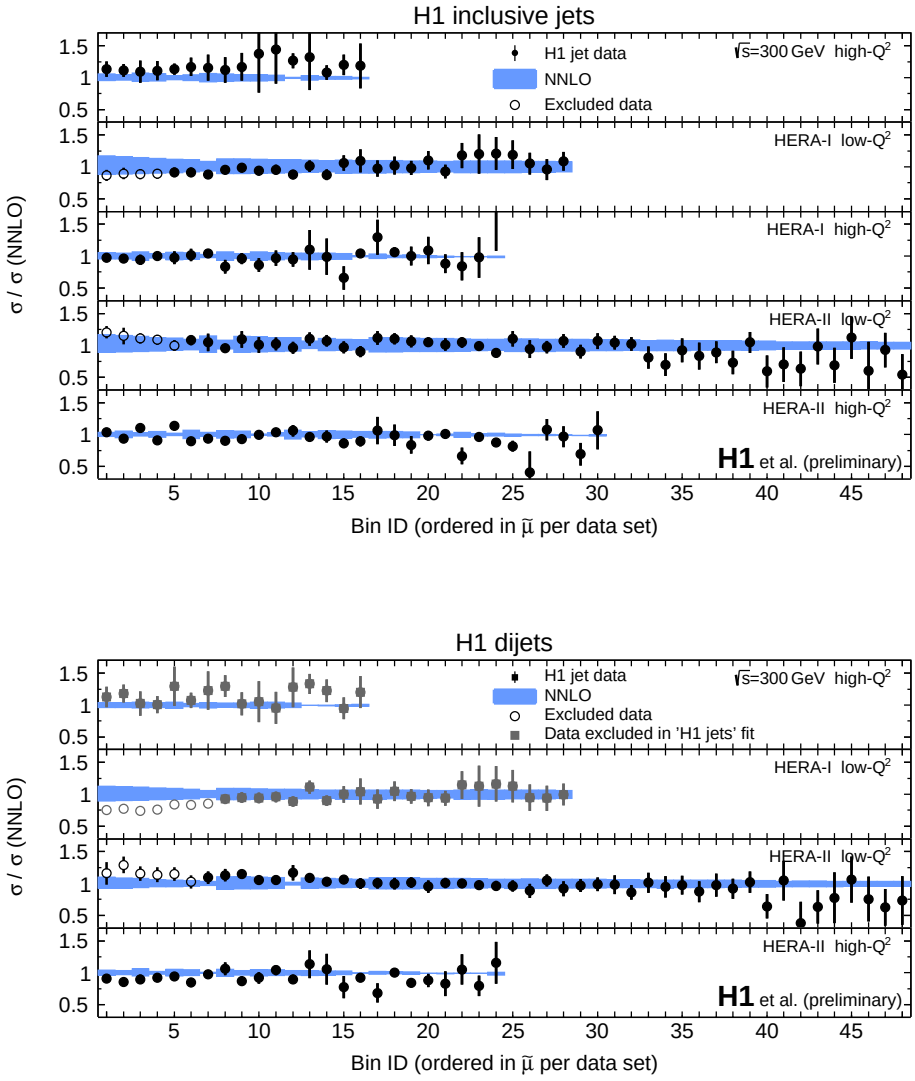

Figure 14: Ratio of inclusive jet (upper panel) and dijet cross sections (lower panel) to NNLO predictions obtained with the best-fit value of $\alpha_s(m_Z)$. The shaded area indicates the uncertainty on the NNLO calculations from scale variations. The open circles show data points, which are not considered for the fits, because their values $\tilde{\mu}$ is below $2m_b$. In case of HERA-I dijets, additional data points are excluded, as these impose symmetric cuts on jet1 and jet2 and thus the NNLO calculations are infrared sensitive. The grey (square) data points are not considered for the 'H1 jets'-fit, since the statistical correlations to the respective inclusive jet measurements are not known.